A robust nanoscale experimental quantification of fracture energy in a bilayer material system

Denvid Lau[a,b], Kurt Broderick[c], Markus J. Buehler[a,1], and Oral Büyüköztürk[a,1]

[a]Department of Civil and Environmental Engineering and [c]Microsystems Technology Laboratories, Massachusetts Institute of Technology, Cambridge, MA 02139; and [b]Department of Architecture and Civil Engineering, City University of Hong Kong, Kowloon, Hong Kong

Edited* by John W. Hutchinson, Harvard University, Cambridge, MA, and approved July 17, 2014 (received for review February 15, 2014)

Accurate measurement of interfacial properties is critical any time two materials are bonded—in composites, tooth crowns, or when biomaterials are attached to the human body. Yet, in spite of this importance, reliable methods to measure interfacial properties between dissimilar materials remain elusive. Here we present an experimental approach to quantify the interfacial fracture energy Γ_i that also provides unique mechanistic insight into the interfacial debonding mechanism at the nanoscale. This approach involves deposition of an additional chromium layer (superlayer) onto a bonded system, where interface debonding is initiated by the residual tensile stress in the superlayer, and where the interface can be separated in a controlled manner and captured in situ. Contrary to earlier methods, our approach allows the entire bonded system to remain in an elastic range during the debonding process, such that Γ_i can be measured accurately. We validate the method by showing that moisture has a degrading effect on the bonding between epoxy and silica, a technologically important interface. Combining in situ through scanning electron microscope images with molecular simulation, we find that the interfacial debonding mechanism is hierarchical in nature, which is initiated by the detachment of polymer chains, and that the three-dimensional covalent network of the epoxy-based polymer may directly influence water accumulation, leading to the reduction of Γ_i under presence of moisture. The results may enable us to design more durable concrete composites that could be used to innovate transportation systems, create more durable buildings and bridges, and build resilient infrastructure.

molecular mechanics | bimaterial systems | superlayer | energy release | biomedical

Interfaces exist whenever materials are bonded together and can be found frequently in both natural and synthetic bonded systems, for instance, the mineral–protein interfaces in animals, interfaces between different phases in composite materials, the enamel–polymer interfaces involved in dental treatment, or the cell–substrate interfaces in biomedical applications (1–7). The integrity of the interface under various environmental conditions—including different temperature and moisture levels—is critical to many applications (8–10). Meanwhile, because of the advancement and development in technology, a large number of bonded systems in various engineering applications are needed, possessing increasingly higher accuracy in design and manufacturing process in a very small length scale. However, currently, a robust and generally applicable methodology to quantify the fracture energy at these interfaces from a microscopic perspective is lacking.

Several straightforward measurement methods for quantifying the interfacial fracture energy on large specimens, such as direct peel/shear specimen (11, 12), Brazilian disk specimen (13), and sandwiched beam specimen (14, 15), have been reported. However, it has been difficult to directly measure this parameter for microscale specimens, such as thin film systems. This is because significant errors in measurement may result from using the above methods due to the complex elastic/plastic stress fields involved. In particular, the applied force on the thin layer during experimentation creates significant plasticity in the vicinity of the crack tip. Here, we introduce an approach called superlayer test in which direct debonding due to the externally applied driving force (in the form of residual tensile effect) with high fidelity can be achieved. This approach involves the use of high residual stress generated during the deposition of metallic materials, which leads to a steady-state loading on a thin film system at the mode mixities relevant to thin film and substrate. For typical thin films ($h < 1$ μm) and representative residual stresses ($\sigma_R \sim 100$ MPa), the induced energy release rate is generally below the interface fracture energy of bonded systems with dimensions of practical interest. Thus, a procedure that substantially increases the steady-state energy release rate, G_{ss}, is required. Such a procedure involves the deposition of a metallic layer, called the superlayer, that increases the effective film thickness and also elevates the residual stress. The superlayer should be selected in accordance with the following four characteristics: (*i*) the deposition can be conducted at ambient temperature, (*ii*) the superlayer should not react with the existing film, (*iii*) it should have good adhesion, and (*iv*) the superlayers can be subjected to a large residual tension upon deposition. Chromium (Cr) film, deposited by electron beam evaporation, meets all four criteria (16). The superlayer test should ultimately allow a robust characterization of interface fracture energy and monitoring scheme of the debonding process while the thickness of the superlayer is increasing. This technique was originated by Bagchi et al. (17), and here we successfully extend its applicability to construction-related material systems. This paper addresses interface applications found primarily in construction materials, including advanced composite materials consisting of organic (e.g., epoxy, fibers, matrix) and inorganic (e.g., brick, concrete, masonry)

Significance

Accurate measurement of interfacial properties is critical any time two materials are bonded—in composites, tooth crowns, or when biomaterials are attached to the human body. Yet, in spite of this importance, reliable methods to measure interfacial properties between dissimilar materials remain elusive. Here we present an experimental method for robust characterization of organic–inorganic interfaces. Combining theory, experiment, and molecular simulation, we show that debonding between layers of materials can be controlled through residual stresses in a deposited metallic layer. We validate the method and show that moisture degrades the bonding between epoxy and silica, a technologically important interface. This may enable us to design more durable concrete composites that could be used to innovate our nation's aging infrastructure.

Author contributions: D.L., M.J.B., and O.B. designed research; D.L., M.J.B., and O.B. performed research; D.L. and K.B. contributed in the experimental program; D.L., M.J.B., and O.B. analyzed data; and D.L., M.J.B., and O.B. wrote the paper.

The authors declare no conflict of interest.

*This Direct Submission article had a prearranged editor.

[1]To whom correspondence may be addressed. Email: mbuehler@mit.edu or obuyuk@mit.edu.

This article contains supporting information online at www.pnas.org/lookup/suppl/doi:10.1073/pnas.1402893111/-/DCSupplemental.

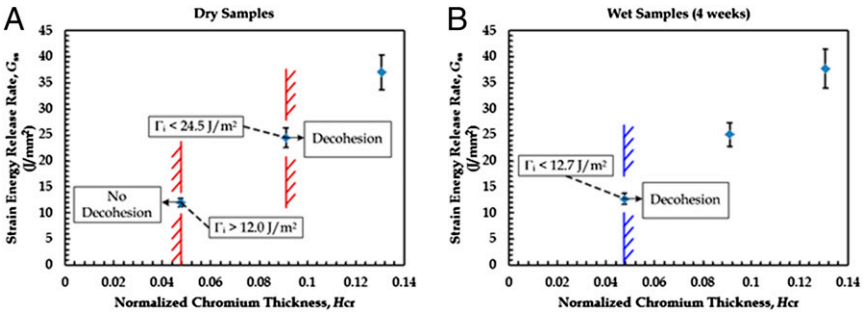

Fig. 1. Two plots of the calculated energy release rates with the normalized Cr layer thickness. (*A*) The red lines show the lower and upper bounds that the critical energy release rate of the epoxy–silica bonded system in dry condition. (*B*) The blue lines show the upper bound of the critical energy release rate of the epoxy–silica bonded system after 4 weeks of moisture conditioning.

components with interfacial fracture energy below 50 J/m^2 as encountered in such material systems.

Results and Discussion

To demonstrate the applicability of this experimental approach, epoxy–silica interface is used as an example, and its interfacial fracture energy (Γ_i) is characterized under both dry and wet conditions. The epoxy–silica interface is fabricated using a silicon wafer with a thermal oxide layer coated by a 20-μm-thick SU-8 film (a type of epoxy commonly used in microfabrication); the results of Γ_i under moisture effect are summarized in Fig. 1. For the dry specimens, the bilayer remained attached to the substrate when the Cr superlayer was 1 μm thick. Conversely, when the Cr layer was either 2 μm or 3 μm thick, debonding occurred, followed by curling of the film as shown in Fig. 2. Consequently, the critical thickness of superlayer, h_c, was between 2 μm and 3 μm for the dry specimens. For the wet specimens, debonding occurred, followed by curling of the film, for all three tested Cr thickness (1 μm, 2 μm, and 3 μm), and hence h_c is less than 1 μm for the wet specimens. After determining these values, together with the measured residual stresses, bounds for the interfacial fracture energy can be calculated. The details are given in *Methods*. At the critical point when interfacial fracture is initiated, Γ_i is equal to the steady-state energy release rate (G_{ss}). Hence, by varying the thickness of the superlayer, various theoretical G_{ss} can be calculated, and by observing if debonding is initiated under the chosen thicknesses, bounds can be placed on the interfacial fracture energy.

For this purpose, the elastic modulus of the film is needed. Generally, polycrystalline thin films can have a lower modulus than the bulk material, because of porosity at the boundaries of the columnar grains. Although we determined the Young's modulus of SU-8 (E_2) using the nanoindentation approach, literature values of polycrystalline Cr thin films (E_1 = 93 GPa) are used here instead because the variation of E_1 under the concerned experimental conditions is very small (18). With the chosen E_1 and E_2, the bounds on the interfacial fracture energy are 12.0 J/m^2 ≤ Γ_i ≤ 24.5 J/m^2 for the dry specimens as shown in Fig. 1*A*. For the wet specimens, only the upper bound can be found based on the chosen Cr thicknesses (1 μm, 2 μm, and 3 μm), and the results show that Γ_i ≤ 12.7 J/m^2 as shown in Fig. 1*B*.

With a higher-resolution SEM image, we observe that the interfacial crack does not separate SU-8 and silica in a clean manner; instead, some hair-like structures connect SU-8 and silica at the vicinity of the crack tip as shown in Fig. 3. These hair-like structures can be observed in both dry and wet specimens. Such observation can validate that the debonding between epoxy and silica is initiated by detachment of the epoxy polymer chain from the silica substrate. When debonding occurs, hair-like structures are formed at the vicinity of the crack tip. In wet conditions, water molecules can seep into the gaps generated by the hair-like structures and eventually weaken the adhesion at the interface as reported in a recent study of the interfacial integrity between a single polymer chain and a silica substrate, using molecular modeling (19, 20). An earlier study of concrete–epoxy interfaces indicated that Γ_i usually ranged between 10 J/m^2 and 20 J/m^2 for the dry case and between 5 J/m^2 and 10 J/m^2 for the wet case (21). Such consistency implies that using silica as a substitute for concrete is a reasonable approach in the modeling and simulation process. The measured interfacial fracture energies between the epoxy–silica system and the epoxy–concrete system are close to each other, probably because the nature of the interfacial bonding of these two systems is similar, dominated by the nonbonded and nondirectional van der Waals forces and Coulombic interaction. In view of the observed hair-liked structures at the epoxy–silica interface, a molecular model, which is capable of describing the debonding mechanism of a single polymer chain attached on a silica surface, is constructed for quantifying the effect of water molecules on the adhesion property more accurately.

To complement the experimental work, interfacial debonding is simulated using an atomistic model. Metadynamics (22, 23) is applied to study the adhesion between diglycidyl ether of bisphenol A (DGEBA) and silica. This algorithm can be used to reconstruct the free-energy landscape by accelerating the sampling of rare events in the system. In particular, it has been demonstrated that this technique can be used to measure the free-energy landscape as a function of the distance between the mass center of a polymer chain structure and silica surface as shown in Fig. 4*A* (20, 24). The converged free-energy landscape is observed when the simulation time is 100 ns for both dry and wet scenarios, and provides the physical energy landscape of the adhesion between DGEBA and silica as a function of the distance as shown in Fig. 4*B*.

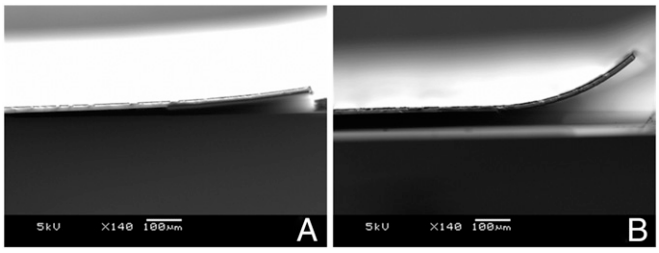

Fig. 2. SEM of the epoxy–silica bonded system with Cr superlayer. (*A*) Interfacial debonding was not observed when the Cr thickness was 1 μm in the dry sample. (*B*) Interfacial debonding was clearly observed with 1-μm-thick Cr superlayer in the wet sample (moisture conditioned for 4 weeks).

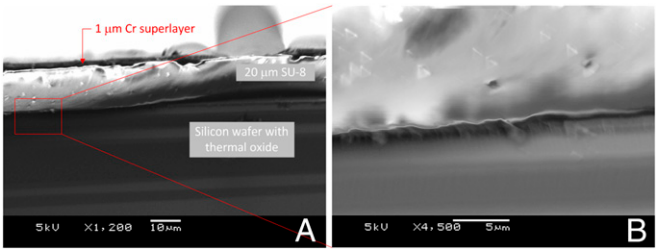

Fig. 3. (*A*) SEM of the epoxy–silica interface at the vicinity of the crack tip. (*B*) Hair-like structures linking the SU-8 and silica are found at the vicinity of the crack tip.

The simulation results show that the depth of energy barrier in the wet scenario (10.2 kcal/mol) is only about one third of that in the dry scenario (31.8 kcal/mol). This result agrees very well with the experimental measurement using the superlayer approach. A possible scenario to explain these differences is that the space surrounding the hair-like structures allows for the accumulation of water molecules. Based on our prior work, it is noted that the adhesion between polymer and silica can be weakened when the polymer is surrounded by water molecules (19). By carefully observing the entire simulation, it is noted that water molecules seep into the gap between the polymer chain and the substrate. When focusing on the nanoscale, our model can mimic the debonding mechanism in both the dry and wet scenarios by capturing the formation of hair-like structures through the peeling and shearing of the polymer chain tail on the substrate surface. This implies that the debonding mechanism, which is initiated by the detachment of a finite amount of polymer chains, is hierarchical in nature, and the three-dimensional covalent network of the epoxy-based polymer may have influence on the water accumulation, leading to the reduction of interfacial fracture energy under the effect of moisture. It is noted that similar hair-like structures have also been reported in the dental research field, and this common observation further implies that the fracture process along the interface can drive material transformation from a continuum to a discrete nature via a series of hair structures. It is likely that this mechanism occurs within the fracture process zone (25). This paper is believed to be the first attempt to explain the moisture degradation using both experimental and simulation technique at a closer length scale, leading to the observation of the continuum-discrete transformation at the fracture initiation state.

It should be emphasized that the superlayer approach reported here can be used in a range between 1 nm and 10 μm and has advantages over various conventional fracture tests. For instance, peeling approaches may create a significant plasticity in the thin film due to an enormous bending effect, and nanoindentation approaches may create a significant plastic deformation at the indenter tip. Such plasticity can hardly be separated from the fracture process and may lead to an inaccurate measurement of fracture energy. We also believe that the approach can be used with adequate accuracy for measuring the interfacial fracture energy of metal-related interfaces, in which the plastic zone cannot be avoided. Using this method, a better accuracy may be achieved compared to some existing fracture testing approaches such as microscratching tests, peel test, Blister tests, and mixed mode fracture tests, because, in this case, the plasticity may be confined to a limited plastic zone in the vicinity of the crack tip. The newly developed approach involves preparation of testing samples; a great number of small specimens can be coated by Cr simultaneously by sputtering, and hence a higher accuracy and a smaller standard deviation of the measured interfacial fracture energy can be achieved.

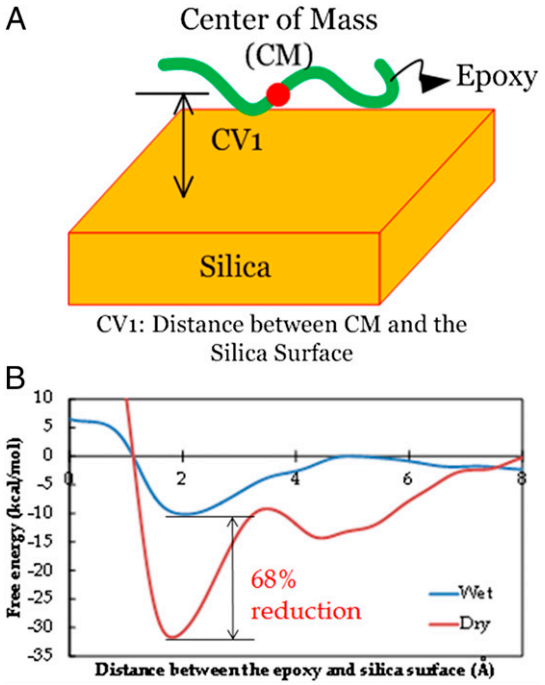

Fig. 4. (*A*) Schematic diagram showing the definition of CV1 in epoxy–silica system. (*B*) It shows the free-energy landscapes of the epoxy–silica system in the dry and wet scenarios. The fracture energy of the system can be calculated by measuring the depth of the energy barrier.

Conclusion

Here we developed a superlayer experimental approach for quantifying the interfacial fracture energy at the nanoscale. We have demonstrated the applicability of this experimental technique on organic–inorganic interface by using epoxy (SU-8) and silica as an example. It was found that one can accurately quantify the interfacial fracture energy, while the debonding process can be observed in situ through scanning electron microscope images, and that moisture has a significant effect on the interfacial fracture energy of the epoxy–silica bonded system. The proposed approach using the Cr superlayer enabled us to confine the range of the actual interfacial fracture energy with high fidelity. By considering upper and lower bounds of the

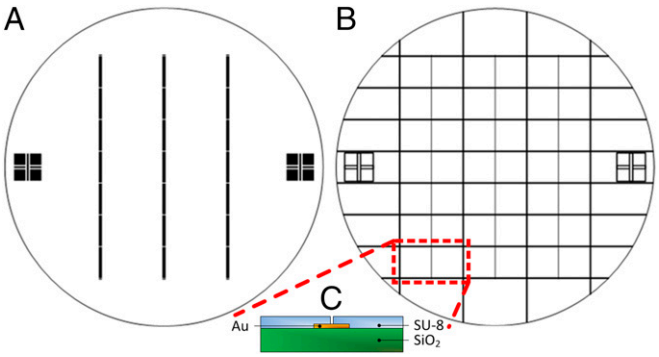

Fig. 5. (*A*) Transparency mask for Au pattern with three 1-mm-wide vertical black strips. (*B*) Transparency mask for SU-8 pattern with 0.5-mm-wide black darker lines and 0.2-mm-wide black lighter lines. The diameter of both transparencies is 152.4 mm. The wafer was broken into 21 smaller pieces, which were then coated by chromium. The rectangular box with red dashed line indicates the size of the single specimen. (*C*) A schematic cross section of the bonded system after the SU-8 pattern.

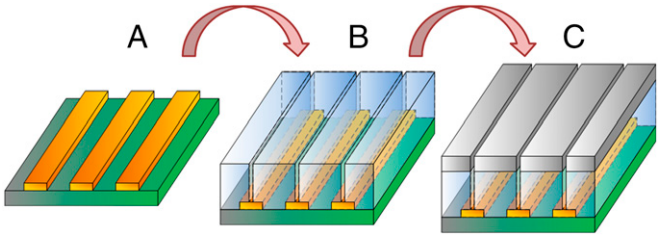

Fig. 6. (*A*) Au pattern on Si wafer with a layer of thermal oxide (0.9 nm). (*B*) SU-8 was spin-coated on the wafer with a thickness of 20 μm. (*C*) Cr was deposited onto the SU-8 surface by the sputterer. The residual tensile stress in Cr leads to the crack initiation at the SU-8–SiO_2 interface when the critical Cr thickness is achieved. This technique was originated by Bagchi et al. (17), and here we have successfully extended its applicability toward construction-related material systems.

interfacial fracture energy for both the dry and wet specimens, we hypothesized that the interface fracture energy of the bonded system can decrease down to 50% of its original value in the presence of water. More importantly, we observe hair-like structures that connect SU-8 and silica at the vicinity of the crack tip, which are formed when the interfacial crack is initiated.

This experimental technique enables us to capture various debonding stages with the increase of the driving force through the increasing deposition depth of the superlayer, can be used from the nano to the micro level, and has advantages for overcoming the plasticity that is generally involved when debonding is initiated by an externally applied force. The developed approach can be widely used in various bilayer material systems, including those found in construction and composite materials as well as metallic and organic-based thin films, provided that a smooth thin film-free surface can be obtained for the deposition of the Cr superlayer. Furthermore, durable concrete material and resilient infrastructure designs can be achieved with the assistance of this robust measurement technique. The experimental quantification introduced could also be useful for nano-/micro-based manufacturing practices, in particular in medical and bioengineering applications, which require an accurate characterization of the interfacial integrity in a bonded material system under different surrounding conditions, such as moist environment.

Methods

Experimental Procedures. In the developed superlayer experimental approach, a silicon wafer with an oxide layer and an epoxy-based polymer (SU-8) were used. Silicon (Si) is a blue-gray, brittle, chemical element in the same group as carbon (C). At 27.8%, it is second only to oxygen (O) as the most common element on the surface of the earth. Silicon is the main ingredient of glass, quartz, soil, and sand. It contributes to hardness and structural strength in many metals such as aluminum–silicon alloy and bronze. The majority of semiconductors and microchips are built on silicon. Before a semiconductor can be built, silicon must be transformed into a wafer. This begins with the growth of a silicon ingot. A single silicon crystal is a solid composed of atoms arranged in a three-dimensional periodic pattern that extends throughout the material. Because silica is the interest of this study, silicon wafers with a 0.9-μm-thick thermal oxide were used. The thermal oxide layer is also crystalline in nature with [1 0 0] orientation. The diameter of the silicon wafer used here was 100 mm, with a thickness of 525 μm.

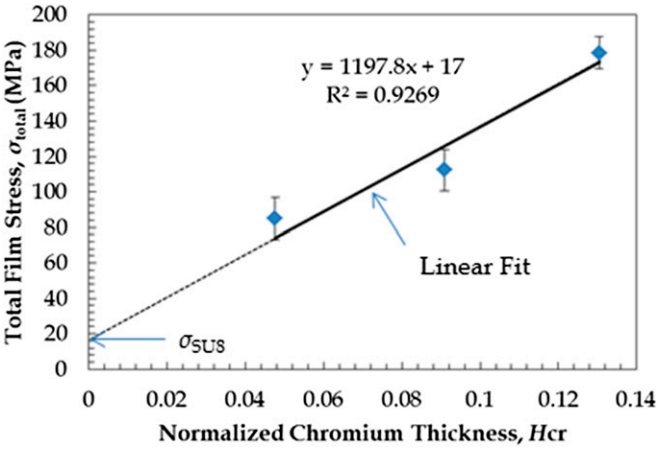

Fig. 7. A plot of the total film stress with the normalized Cr layer thickness.

The experiment relies mainly on measuring the curvature of the thin film system using profilometer. Based on the curvature measurement, the stress in the film can be calculated with the associated standard deviation. With the calculated stress, the interfacial fracture energy can be quantified accordingly. Deposition and photolithography were conducted. Residual stresses were measured from beam deflections using the mechanical surface profilometer. Then, film severing above the precrack is conducted. The films were inspected to assess the critical thickness, h_c, using SEM. Finally, the interfacial fracture energy was determined by the measurement of this critical thickness.

The fabrication of the specimen to be used for the superlayer test involves two major steps: (*i*) gold (Au) patterning on silica for creating precrack regions and (*ii*) SU-8 patterning with the preexistence of Au. The choice of SU-8 is particularly attractive due to its emerging importance as an adhesive that is usually used in various engineering fields including microelectromechanical systems, optics, and bioengineering. Careful substrate cleaning is essential. For this purpose, the silica substrate (silicon wafer with thermal oxide) was solvent cleaned in trichloroethylene, acetone, and isopropyl alcohol in order to remove organic contaminants. Then, the wafer was water cleaned, followed by etch cleaning in buffered hydrofluoric acid, in order to remove all inorganic contaminants. Finally, the wafer was rinsed in deionized water and dried by putting it on the 105 °C hot plate for 10 min. In order to achieve the Au pattern, a negative photoresist (AZ5214) was first coated onto the silicon wafer with thermal oxide using a spin coater with a speed of 3,000 rpm for 30 s. After that, the wafer was soft-baked with compression on a 105 °C hot plate for 3 min. Then, the wafer was exposed under ultraviolet (UV) light for 20 s using a hard contact approach with the transparency mask shown in Fig. 5*B*. It should be mentioned that the hard contact approach involves a clean glass plate and a transparency mask placed on top of the wafer. Postexposure baking was conducted on a 105 °C hot plate for another 3 min, followed by flood exposure under UV light for another 1 min without the transparency mask, which is regarded as soft contact. Finally, the negative photoresist was developed in AZ422 for 1 min, followed by rinsing using deionized water. Au layer (thickness ~30 Å) was then deposited onto the negative photoresist patterned wafer by electron beam evaporation. The Au pattern was achieved by removing the AZ5214. The stripper for the AZ5214 used to "lift off" the Au was an n-methyl-2-pyrrolidone-based solution. The obtained Au pattern acts as the precrack region for the epoxy–silica bonded system.

After achieving the Au pattern, SU-8 was coated on Au strips using spin coater. SU-8 2015 was spin-coated onto the Au patterned wafer using a speed 3,000 rpm for 30 s. After that, the wafer was soft-baked on a 95 °C hot plate for 5 min. Then, the wafer was exposed under UV light for 45 s using a hard contact approach with the transparency mask shown in Fig. 5*B*. It should be mentioned that the solid and hollow square symbols shown in Fig. 5 are for aligning purpose during the patterning process. Postexposure bake was conducted on a 95 °C hot plate for another 5 min. Finally, SU-8 was

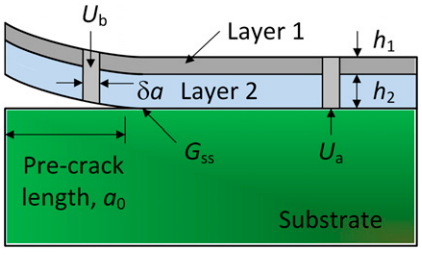

Fig. 8. Schematic diagram showing the energy balance approach to find the strain energy release rate for a bilayer thin film system.

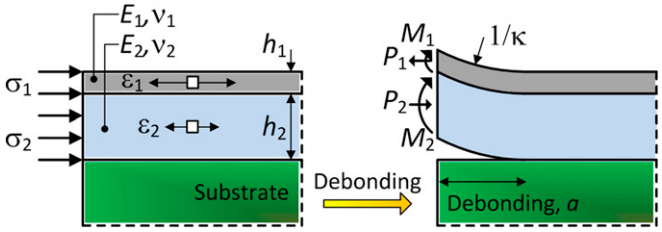

Fig. 9. Schematic diagram showing the deformation of a bilayer thin film system when subjected to residual tensile stresses, resulting in interfacial debonding. The stresses σ_1 and σ_2 are the misfit stresses in the Cr (subscript $I = 1$) and SU-8 (subscript $I = 2$), which provide the forces, P_i, and the moments, M_i, in the bilayer thin film system above the debonding region. The curvature of the debonded bilayer thin film is κ. They are defined as $\sigma_i(z) = P_i/h_i + zM_i/I_i$, $M_i/I_i = E_i'\kappa$, and $I_i = h_i^3/12$, where z denotes the vertical distance from the neutral axis in each layer, and I_i is the sectional modulus.

developed on the spin coater with PM acetate, followed by rinsing in isopropyl alcohol, and the SU-8 pattern was achieved. The schematic cross section of the epoxy–silica bonded system is shown in Fig. 5*C*.

After having prepared the epoxy–silica bonded system through the above procedure, the wafer was broken into smaller specimens for the chromium deposition. Each wafer could generate 21 specimens, as shown in Fig. 5*B* with the red dashed boundary. Eighteen specimens were conditioned in a water bath for 4 weeks, and they were regarded as wet, while another 18 specimens were placed in a 65 °C oven for 2 weeks to minimize the water content in the specimen, and those specimens were regarded as dry. Chromium (Cr) was then deposited by sputterer. Two targets were used during the deposition, and hence the Cr deposition rate of 3 Å/s could be achieved. Three different Cr thicknesses were achieved, namely, 1 μm, 2 μm, and 3 μm. For the thickest superlayer (3 μm), the deposition took about 3 h to complete. Once the critical Cr thickness was reached, the SU-8 debonded from the wafer. The interfacial crack was initiated at the tip of the precrack (Au) and propagated along the interface between SU-8 and the wafer. The entire fabrication process is summarized in Fig. 6.

After fabricating the specimen, the first measurement was made on the quantification of the residual stresses in both SU-8 and Cr layers. The residual stress was measured through a standard procedure that relies on determination of the film/substrate system using the Stoney formula (26). It is noted that the Stoney formula can only work for a continuous thin film bonded system. Here we assume that the stresses in both the Cr and SU-8 are the same before and ahead of the precrack region (where vertical separation exists). In order to make certain that the assumption would not affect the accuracy of the calculation significantly, the length of the precrack (0.5 mm) was chosen to be much smaller than that of the specimen (10 mm) by more than an order of magnitude. In addition, the curvature perpendicular to the crack length was not considered in our calculation, because such curvature would have insignificant effect on driving the crack propagation and the specimen was designed such that one-way bending was dominant. For this purpose, a profilometer is used to measure substrate curvature (27). The profilometer uses a metallic stylus, which is horizontally scanned while its vertical movement is converted to an electrical signal. The substrate often has an initial curvature. Therefore, two scans are made in order to measure the radius of curvature of the substrate. These are made both with and without the film attached. The residual stress in the film is related to the measured radius of curvature by:

$$\sigma_R = \frac{E_s h_s^2 \kappa}{6h_f(1-\nu_s)} \quad [1]$$

where h_s is the substrate thickness, h_f is the film thickness, κ is the curvature, and E_s and ν_s are the substrate Young's modulus and Poisson's ratio, respectively. This procedure is used to evaluate the residual stress in the SU-8 and then the residual stress in the Cr deposited onto the SU-8. The total stress, σ_{total}, associated with both is

$$\sigma_{total} = \sigma_{SU8}H_{SU8} + \sigma_{Cr}H_{Cr} = \sigma_{SU8} + (\sigma_{Cr} - \sigma_{SU8})H_{Cr} \quad [2]$$

where H is the relative thickness, i.e., $H = h/(h_{SU8} + h_{Cr})$. Consequently, if the stresses are essentially independent of the film thicknesses, there would be a linear dependence of the total stress on the relative thickness, H. This approach was used to assess the experimental results.

Residual stress measurements were performed on a batch of three samples with the same nominal SU-8 thickness (20 μm) and with three Cr thicknesses: 1 μm, 2 μm, and 3 μm. On each sample, five profilometer scans were made before and after depositing the film onto the substrate. A least square regression fitting to the data gave the measured radius of curvatures and their respective standard deviations. The film thickness was also obtained from the scans by making small scratches on the coated surface. The level difference measured by the profilometer indicated the film thickness accordingly. The stresses obtained in this manner are plotted in Fig. 7. A linear fit is obtained, consistent with stresses in each separate layer being independent of thin film thickness as shown in Eq. **2**. This fit indicates that the residual stresses in the SU-8 and Cr layers are 17 MPa and 1,248 MPa, respectively, with standard deviations ~5%, and these values are within the range measured by others (17, 28). It is noted that similarities can be seen between Figs. 1, 7, and 8 and comparable figures in ref. 28. However, the approach reported therein is limited to interface systems containing a metal component (such as electronic applications) while the current approach is applicable to various applications of construction and composite materials.

The steady-state energy release rate, G_{ss}, controls the interfacial debonding motivated by residual stresses in the deposited thin film layers when the interfacial flaw size, a_0, exceeds the film thickness. Moreover, since the film stress diminishes upon occurrence of the interfacial debonding, the energy release behavior is entirely elastic. For the thin film system as shown in Fig. 8, G_{ss} can be calculated by considering the strain energy far ahead and far behind the growing interfacial crack. It should be mentioned that the interfacial crack in the thin film/substrate system is propagating under the plain strain condition. If U_a and U_b denote the strain energies in the two volume elements having the width Δa as shown in Fig. 8, then

$$G_{ss} = \frac{U_a - U_b}{\Delta a}. \quad [3]$$

For a bilayer, the strain energy far ahead of the crack tip is the sum of the elastic strain energy associated with each layer (SU-8 and Cr) and can be written as:

$$U_a = \sum_i U_a^i = \left(\frac{\sigma_1^2 h_1}{E_1'} + \frac{\sigma_2^2 h_2}{E_2'}\right)\Delta a. \quad [4]$$

Fig. 9 shows the free-body diagram of the bilayer thin film system corresponding to the situation when both layers are under residual tensile stresses. The film bends upward after decohesion in order to release the strain energy. The resultant stresses in each layer can be related to the forces (P_i), moments (M_i), and curvature (κ) defined in Fig. 9, and the strain energy far behind the crack tip can be written as:

$$U_b = \sum_i \frac{1}{E_i'}\left(\frac{P_1^2}{h_i} + \frac{M_i^2}{I_i}\right)\Delta a. \quad [5]$$

At this stage, it is required to link up P_1, P_2, M_1, M_2, and κ to the residual tensile stresses (σ_1 and σ_2) and the film thickness (h_1 and h_2), which are the known parameters. This procedure involves five linear equations with five

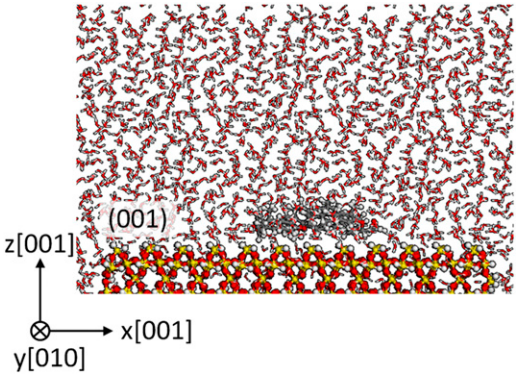

Fig. 10. Snapshot of the model showing a DGEBA polymer chain attached onto a (001) silica substrate with yellow dots (silicon), red dots (oxygen), and white dots (hydrogen). Water molecules are present in the wet scenario, while they are absent for the study of dry case.

unknowns (*i.e.* P_1, P_2, M_1, M_2, and κ). Two equations are obtained from the consideration of force and moment equilibrium. Another two equations are obtained from the consideration of geometry between the moments and the curvature. Finally, by considering the strain compatibility at the interface between Cr (subscript $i = 1$) and SU-8 (subscript $i = 2$), one more equation can be obtained. Hence, an analytical solution for P_1, P_2, M_1, M_2, and κ can be evaluated, and, eventually, the steady state-energy release rate can be solved accordingly.

Molecular Modeling. To complement the experimental work, interfacial debonding is simulated using an atomistic model. DGEBA is one of the major epoxy types and the main component found in SU-8. The adhesion between DGEBA and silica is the focus of this model. We use a consistent valence forcefield (CVFF) to describe the interactions of atoms, where the total potential energy of the system is composed of bonding, angular, dihedral, improper, and pair potential including a 12-6 Lennard–Jones potential and Coulombic interactions. We extended the CVFF parameter files (29) to describe the interactions of atoms within DGEBA and between DGEBA and silica, together with the CVFF water potential, a three-site model with internal geometry corresponding to the gas-phase experimental structure (30). Flexibility of water molecules is modeled through the use of harmonic bond stretching and angle bending potentials. Our simulation box includes a silica slab with its top surface corresponding to α-quartz (001) surface in contact with DGEBA molecule as shown in Fig. 10, fully surrounded by water molecules in the wet scenario. Periodic boundary conditions are applied in all directions, and dimensions of the simulation box are large enough beyond the simulation cutoff to ensure that the interactions between mirror solutes are minimal. The system is equilibrated for 1 ns in an NPT (number/pressure/temperature) ensemble, i.e., constant number of particles, constant pressure (1 atm), and constant temperature (300 K), and energy and root-mean-square deviation calculations are performed to ensure that an equilibrium state is reached. The metadynamics simulations are then performed by LAMMPS and the PLUMED packages (31, 32). The external energy in a Gaussian distribution with a height 0.005 kcal/mol and width 0.35 Å is deposited into the system every 100 fs.

ACKNOWLEDGMENTS. This research was supported by the National Science Foundation through Grant CMS-0856325.

1. Moffat KL, et al. (2008) Characterization of the structure-function relationship at the ligament-to-bone interface. *Proc Natl Acad Sci USA* 105(23):7947–7952.
2. Qin Z, Buehler MJ (2012) Cooperativity governs the size and structure of biological interfaces. *J Biomech* 45(16):2778–2783.
3. Stavis C, et al. (2011) Surface functionalization of thin-film diamond for highly stable and selective biological interfaces. *Proc Natl Acad Sci USA* 108(3):983–988.
4. Tao C, et al. (2008) Dynamic interfaces in an organic thin film. *Proc Natl Acad Sci USA* 105(43):16418–16425.
5. Xu Z, Buehler MJ (2010) Interface structure and mechanics between graphene and metal substrates: A first-principles study. *J Phys Condens Matter* 22(48):485301.
6. Xu Z, Buehler MJ (2012) Heat dissipation at a graphene-substrate interface. *J Phys Condens Matter* 24(47):475305.
7. Yin Y, Alivisatos AP (2005) Colloidal nanocrystal synthesis and the organic-inorganic interface. *Nature* 437(7059):664–670.
8. Kendall K (1994) Adhesion: Molecules and mechanics. *Science* 263(5154):1720–1725.
9. Cristescu R, et al. (2009) Thin films of polymer mimics of cross-linking mussel adhesive proteins deposited by matrix assisted pulsed laser evaporation. *Appl Surf Sci* 255(10): 5496–5498.
10. Ho PS (1989) Chemistry and adhesion of metal-polymer interfaces. *Appl Surf Sci* 41-42: 559–566.
11. Au C, Büyüköztürk O (2006) Peel and shear fracture characterization of debonding in FRP plated concrete affected by moisture. *J Compos Constr* 10(1):35–47.
12. Tuakta C, Büyüköztürk O (2011) Deterioration of FRP/concrete bond system under variable moisture conditions quantified by fracture mechanics. *Composites, Part B* 42(2):145–154.
13. Hutchinson JW (1990) Mixed mode fracture mechanics of interfaces. *Metal-Ceramic Interfaces*, Acta-Scripta Metallurgica Proceedings Series, eds Ruhle M, Evans AG, Ashby MF, Hirth JP (Pergamon, Oxford), Vol 4, pp 295–306.
14. Büyüköztürk O, Lee K-M (1993) Assessment of interfacial fracture toughness in concrete composites. *Cement Concr Compos* 15(3):143–151.
15. Lee K-M, Büyüköztürk O (1995) Fracture toughness of mortar-aggregate interface in high-strength concrete. *ACI Mater J* 92(6):634–642.
16. Evans AG, Hu MS (1989) The cracking and decohesion of thin films on ductile substrates. *Acta Metall Mater* 37(3):917–925.
17. Bagchi A, Lucas GE, Suo Z, Evans AG (1994) A new procedure for measuring the decohesion energy for thin ductile films on substrates. *J Mater Res* 9(7):1734–1741.
18. Janda M (1986) On the intrinsic stress in thin chromium films. *Thin Solid Films* 142(2): 37–45.
19. Büyüköztürk O, Buehler MJ, Lau D, Tuakta C (2011) Structural solution using molecular dynamics: Fundamentals and a case study of epoxy-silica interface. *Int J Solids Struct* 48(14-15):2131–2140.
20. Lau D, Büyüköztürk O, Buehler MJ (2012) Characterization of the adhesive strength between epoxy and silica using a multiscale approach. *J Mater Res* 27(14):1787–1796.
21. Lau D, Büyüköztürk O (2010) Fracture characterization of concrete/epoxy interface affected by moisture. *Mech Mater* 42(12):1031–1042.
22. Laio A, Gervasio FL (2008) Metadynamics: A method to simulate rare events and reconstruct the free energy in biophysics, chemistry and material science. *Rep Prog Phys* 71(12):126601.
23. Laio A, Parrinello M (2002) Escaping free-energy minima. *Proc Natl Acad Sci USA* 99(20):12562–12566.
24. Qin Z, Buehler MJ (2012) Molecular mechanics of dihydrozyphenylalanine at a silica interface. *Appl Phys Lett* 101:083702.
25. Tamse A (1988) Iatrogenic vertical root fractures in endodontically treated teeth. *Endod Dent Traumatol* 4(5):190–196.
26. Stoney GG (1909) The tension of metallic films deposited by electrolysis. *Proc R Soc Lond A* 82(553):172–175.
27. Thomas ME, Hartnett MP, Mckay JE (1988) The use of surface profilometers for the measurement of wafer curvature. *J Vac Sci Technol A* 6(4):2570–2571.
28. Abermann R (1992) *Thin Films: Stresses and Mechanical Properties III*. Materials Research Society Symposium Proceedings, eds Nix WD, Bravman JC, Arzt E, Freund LB (Mater Res Soc Symp Proc 239, Pittsburgh), pp 213–256.
29. Dauber-Osguthorpe P, et al. (1988) Structure and energetics of ligand binding to proteins: *Escherichia coli* dihydrofolate reductase-trimethoprim, a drug-receptor system. *Proteins* 4(1):31–47.
30. Lau KF, Alper HE, Thacher TS, Stouch TR (1994) Effects of switching functions on the behavior of liquid water in molecular dynamics simulations. *J Phys Chem* 98(35): 8785–8792.
31. Bonomi M, et al. (2009) PLUMED: A portable plugin for free-energy calculations with molecular dynamics. *Comput Phys Commun* 180(10):1961–1972.
32. Plimpton S (1995) Fast parallel algorithms for short-range molecular dynamics. *J Comput Phys* 117(1):1–19.